REDUCING PROTOTYPE FABRICATION TIME THROUGH ENHANCED MATERIAL EXTRUSION PROCESS CAPABILITY

Parry, Georgia Rose;
Felton, Harry James;
Ballantyne, Robert;
Su, Shuo;
Hicks, Ben

University of Bristol

ABSTRACT

3D printing is a widely used technology for automating the fabrication of prototypes. The benefits are wide reaching, and include low required expertise, accurate geometric form and the processibility of many materials. However, production of certain forms – especially large forms – can be slow. From review of the sub-systems, the hotend is commonly found to be the limiting factor. To improve this, a modified nozzle design is considered that incorporates a flat copper plate within the flow stream. Analytical simulation was used to guide this design before experimental methods validated the modifications. The maximum volumetric rate for the standard hotend nozzle is 14 mm3/s. The best performing modified nozzle increased the maximum volumetric flow rate to 26 mm3/s – an 86% increase. A series of popular parts were further considered, demonstrating a maximum ~48% fabrication time reduction, and a mean of ~23%. This enables 3D printed prototypes to be made more efficiently – both with regards to the design cycle and energy use – and allows designers to use the technology more rapidly than previously possible. By extension, this improves the efficiency of the design process.

Keywords: Prototyping, 3D printing, Additive Manufacturing, New product development

Contact:
Felton, Harry James
University of Bristol
United Kingdom
harry.felton@bristol.ac.uk

Cite this article: Parry, G. R., Felton, H. J., Ballantyne, R., Su, S., Hicks, B. (2023) 'Reducing Prototype Fabrication Time through Enhanced Material Extrusion Process Capability', in *Proceedings of the International Conference on Engineering Design (ICED23),* Bordeaux, France, 24-28 July 2023. DOI:10.1017/pds.2023.303

1 INTRODUCTION

Additive Manufacturing (AM), often referred to as 3D printing and rapid prototyping, is the overarching name for the process of joining materials to fabricate parts from 3D model data, usually layer upon layer (BSI, 2021). Material Extrusion (MEX) printing is an evolved branch of 3D printing, in which material is dispensed through a nozzle or orifice (BSI, 2021). It is the most popular form of 3D printing with 95% of operators using this process in 2021 (Sculpteo, 2021). Although by far the most widely used AM technology, its primary use is as a means of prototype fabrication rather than production. A 2021 industry survey found that 82% of all 3D printer operators utilise AM as a means for prototype fabrication (Sculpteo, 2021), with 48% stating that building of the prototype is where the greatest timesaving can be realised (Sculpteo, 2020). Such time savings are possible because of the ability to fabricate geometrically complex prototypes at relatively low cost and with a high level of automation (Felton, Yon and Hicks, 2020) meaning that fabrication can be performed overnight and unsupervised. Despite these capabilities, the sometimes lengthy fabrication times can induce design fixation (Youmans, 2011; Camburn *et al*., 2017), which in turn affects the speed of design iteration. As such, it is proposed that despite the high levels of automation, there remains a need to accelerate the fabrication rate of MEX printers to further accelerate the design process.

To improve efficiency of the MEX fabrication process, conventional MEX systems were reviewed, with literature identifying the limiting system as the hotend (Mackay, 2018). As such, the hot end was identified as the primary sub-system for further investigation. This work aims to investigate the feasibility of enabling improvement in the fabrication efficiency (speed and energy cost) of the MEX process through modification to the hotend system, considering application to the fabrication of prototypes within the design process.

Previously proposed designs for decreasing print time through hotend development include using multiple print heads simultaneously (Zhang *et al*., 2018), or multi-stage nozzles which can vary in diameter depending on feature requirements (Brooks, Rennie and Abram, 2020). However, these solutions require extensive changes to current MEX systems. Alternatively, nozzle setup modifications already in existence can be utilized, such as the extended length nozzle and heater block, increasing the melting zone of the hotend (known as the "volcano" setup (E3D, 2022)). Although this set-up requires less modification, the set-up increases printhead size. This reduces the maximum print height, and in turn possible print size, whilst also limiting print speed without motion system upgrades. Alternatively, the Bondtech CHT nozzle splits the filament on entry using a complex internal geometry to improve heat transfer using a standard hotend (Bondtech CHT® Coated Brass Nozzle, no date), a design concept which is licensed from 3D Solex. While beneficial, this solution also requires complex nozzle geometry to be defined.

In order to overcome the compromises and complexity of previously discussed modifications, this paper presents an investigation into the feasibility of a simple nozzle modification on the efficiency of fabrication – both with regards to energy use and print time. Initially a conventional nozzle design is considered for baselining before an updated geometry with a simple splitting plate and increased bore is investigated. Both analytical and experimental analyses were performed, with the intention to determine maximum Volumetric Flow Rate (VFR) and establish a link between the methods. Finally, print time comparisons between the conventional and modified nozzles are compared for a series of popular printed parts to assess the modifications feasibility. It should be noted that this work is intended as a feasibility study and proof-of-concept demonstration, not as a design study; though this may be an appropriate extension.

2 NOZZLE GEOMETRY

This work is based on a Prusa i3 MK3S printer – a widely used desktop size MEX machine (Prusa Research, 2021). Standard 0.4 mm brass nozzles were used, with geometry consistent of that used in many of the most widely used machines (E3D, 2022). PLA was chosen as the printing medium as it required the lowest extruder temperature and is a common 3D printing material for prototyping (Hallgrimsson, 2012; Redwood, Schöffer and Garret, 2017). As such, the proposed changes were considered for the most common use case but should be highly generalisable to further machines and materials.

For the purpose of this study, five nozzle combinations were designed and manufactured that used a copper insert, of either 0.55- or 0.7-mm thickness, and enlarging of the nozzle channel (referred to

https://doi.org/10.1017/pds.2023.303 Published online by Cambridge University Press

herein as “bore”). The combinations were then denoted as standard, 0.55 mm no bore, 0.55 mm bore, 0.7 mm no bore, and 0.7 mm bore. Splitting of the geometry into two semi-circles resulted in more efficient geometric shapes (reduced distance to the centre and increased ratio of circumference to area) and hence a reduction in required heating time was expected. To improve the physical efficiency of the flow, the insert top faces were chamfered using a file to an edge to allow the filament to be split more easily. Testing of each design combination allowed the comparison of the different parameters and their effect on the flow rate. The copper insert, see Figure 1a, was located at the upper portion of the nozzle extending from the face to depth of 3mm – the modification to the nozzle was performed using electronic discharge machining. An example of the modified nozzle is shown in Figure 1b.

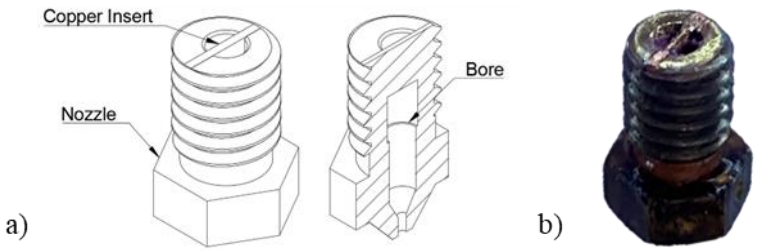

Figure 1. a) Schematic of the modified nozzle designs b) Physical modified nozzle

As previously mentioned, some nozzles were bored out. This was done as the addition of the copper plate resulted in a reduction of the nozzle cross-sectional flow area. The bore size was determined to increase the cross-sectional area to be equivalent to that of the standard nozzle.

3 ANALYTICAL MODELLING OF MEX HEATING PROCESS

The analytical study was performed using Ansys Fluent to understand the melt dynamics within the nozzle and how physical modifications and inlet feed rate would affect the thermal efficiency of the hotend. Although previous work has considered modelling melt dynamics (Serdeczny, 2020; Prusa Research, 2021; Zhang *et al*., 2021) they are only applicable to a range of shear stresses (Moldex, no date), which is inappropriate for consideration of this work (high-speed feed(Go *et al*., 2017)) (Anderegg *et al*., 2019). Other work has shown that inlet feed rate affects outlet temperature (Go *et al*., 2017; Mishra *et al*., 2021), as expected, but the authors are not aware of any work that determines the VFR and links the analytical and experimental methods.

3.1 Numerical modelling

The modified nozzle geometry shown in Figure 2 was considered in 2D with focus on the central axis (as this was furthest from the heat source). Geometric fit and tolerances were neglected, and it was assumed the filament was directly heated by the nozzle – shown to be appropriate (P.Serdeczny *et al*., no date) . The geometry was meshed using multizone Quad/Tri mesh method within Ansys.

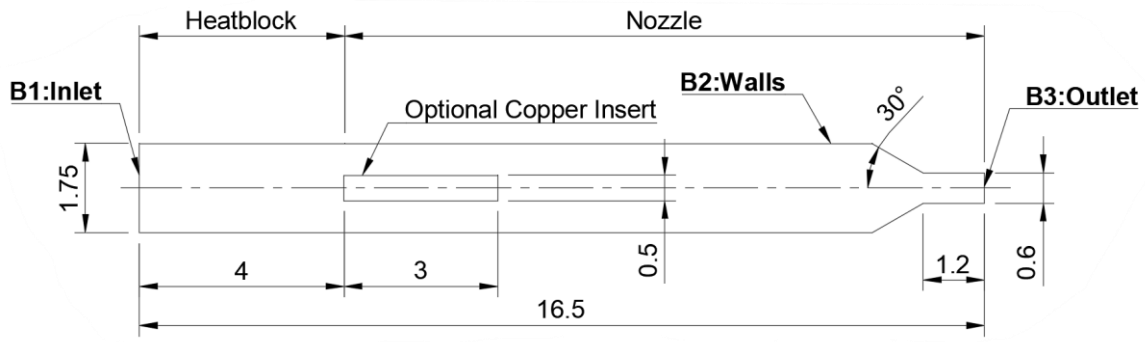

Figure 2. Schematic of modified nozzle geometry used in numerical modelling, dimensions based on manufacturer nozzle and heat block schematics (Sculpteo, 2021) and given in mm.

https://doi.org/10.1017/pds.2023.303 Published online by Cambridge University Press

Momentum and thermal boundary conditions were imposed on the three boundaries indicated on the geometry shown in Figure 2, indicated by B1, B2, B3. The applied momentum boundaries conditions were; velocity magnitude normal to inlet, zero pressure condition at outlet and a stationary wall with a no slip condition - validated in literature (Go *et al*., 2017; Zhang *et al*., 2021). The thermal boundaries at the inlet and outlet were set to room temperature (20˚C). A constant wall temperature of 210 ˚C, the temperature of the heat block was applied and validated to represent the operational conditions(Go *et al*., 2017). This temperature assumption was extended to the internal geometry wall of the modified nozzle. Initial conditions of zero velocity and 210 ˚C filament temperature were used.

To model the filament flow, material properties were applied to the fluid to mimic the behaviour of PLA; a thermoplastic material which displays non-Newtonian and shear thinning characteristics (Hamad, Kaseem and Deri, 2011). The variable viscosity was modelled using Cross-WLF which describes the shear rate dependency across the upper Newtonian region and the shear-thinning region in addition to temperature dependency (Moldex, no date) – shown to be appropriate. The Cross-WLF parameters for PLA were taken from an existing study by Ases Akas Mishra and *et al* (Mishra *et al*., 2021). The thermal conductivity, specific heat capacity and density variation were considered constant throughout as validated by an existing studies (Mishra *et al*., 2021, Phan *et al*., 2020).

A transient model was used to simulate the melt dynamics; monitoring continuity, momentum, energy, and viscosity which allowed for the temperature distribution and its viscosity dependency to be modelled. A laminar flow solver was implemented as the flow was determined to be laminar for the full duration, with all Reynolds numbers being between the magnitudes of $10^{-6} - 10^{-8}\ kg/ms$. A pressure-velocity coupling and second order up-wind spatial schemes were implemented providing more robust and accurate results compared to alternative solvers offered by Ansys (Ansys, no date). VFRs between 2mm^3/s and 50mm^3/s were investigated, with the upper value corresponding to the maximum linear speed of the printer (Prusa Research, 2021). These VFRs approximate to print speeds of 8 mm/s and 200 mm/s, given a layer height of 0.35mm. Ansys' built-in contour function was used to plot the velocity, temperature and viscosity distributions (see Figure 4a for the temperature profile). These were checked against existing studies to validate the magnitudes and distributions (Liang, 2008; Wang, 2012; FilaPrint, no date).

3.2 Failure criteria

To determine the maximum analytical VFR, two failure criteria were defined.

1. Average Output Temperature – The average temperature across the outlet must be equal to or above 145˚C, the melting temperature of the filament (FilaPrint, no date), a condition supported by an existing study (Shaqour *et al*., 2021).
2. Minimum Output Temperature – The minimum temperature across the outlet must be equal to or above, 55˚C, the glass transition temperature of the filament (FilaPrint, no date).

The VFR at which the outlet temperature profile of the nozzle fails to meet both and/or one of these requirements corresponds to the maximum VFR. If the filament is not sufficiently heated, the force required for extrusion increases significantly (Go *et al*., 2017), causing slip in the extrusion system which can no longer produce the required force leading to under extrusion and failure. These failure criteria were confirmed by the relationship between analytical and experimental results for the standard nozzle which is further discussed in Section 5.

3.3 Numerical results

The minimum and average temperatures were recorded for each corresponding VFR and nozzle, plotted in Figure 3c. The maximum VFR was found to be 13 mm^3/s and 26 mm^3/s for the standard and modified nozzle respectively. The corresponding temperature profiles for the standard and modified nozzle at 26 mm^3/s are shown in Figure 3a and 3b respectively.

There was some numerical uncertainty in the introduction of the assumption of constant temperature for the nozzle and insert wall. Due to the small dimensions of the insert this assumption introduces a potential over estimation of the boundary condition and hence the maximum analytical VFR. It was recognised that these boundary conditions would vary depending on conditions outside the control of the study. Given the purpose of this study was to estimate an approximate maximum VFR, they were deemed to be sufficient.

The temperature profile of the maximum VFR shown in Figure 3a illustrates the slow radial conduction of heat to the centre of the filament, as expected due to the low thermal conductivity of

https://doi.org/10.1017/pds.2023.303 Published online by Cambridge University Press

PLA (Mishra *et al*., 2021). Heat conduction is inefficient due to the circular nature of the nozzle and filament. A direct comparison of Figure 3a and 3b demonstrates the significant improvement in heat transfer resulting from the geometry change.

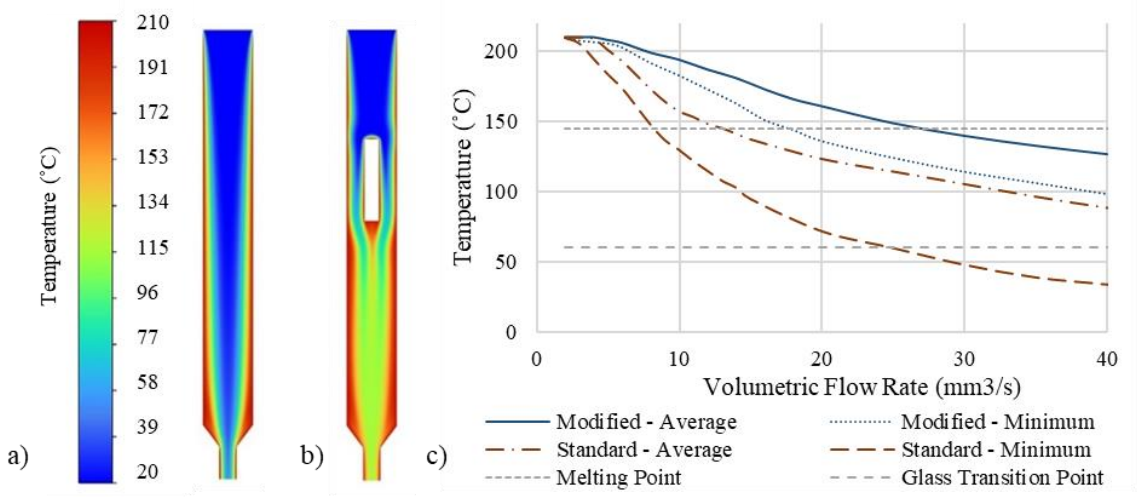

Figure 3. Temperature profile of a) standard nozzle at VFR of 26 mm³/s, b) modified nozzle at VFR of 26 mm³/s, and c) Graph showing average and minimum temperature outlet against VFR.

For the standard nozzle, minor failure will be seen after 13 mm³/s until 25 mm³/s where significant failure would likely occur due to both failure criteria not being met. At this rate a proportion of the filament will not reach the glass transition temperature resulting in significant under extrusion due to flow restriction. The modified nozzle would expect to see small inconsistencies in the print above 26 mm³/s as the glass transition temperature is reached. However, the minimum temperature across the nozzle outlet does not drop below the glass transition point (FilaPrint, no date) within the limits of the printer motion capabilities. Therefore, significant failure of the print due to the hotend subsystem is not expected before limit of the motion system has been reached (Prusa Research, 2021).

4 EXPERIMENTAL TESTING

The relative and absolute performance of the nozzles were determined practically using a series of tests to assess extrusion and print quality. The pure extrusion testing was undertaken to identify how the mass of extruded material compared to that expected at different extrusion rates. The extrusion additionally had several measurements of diameter taken to assess die swelling (Vicente, 2012). Both of these variables effect print quality (Wang, 2012), and so were directly assessed. The second test sought to assess print quality more broadly. This was done by printing continuous paths of material with extrusion rate proportional to the layer being deposited. Print imperfections could therefore be identified for each layer, and therefore extrusion rate. These are each reported in the following sections.

4.1 Pure extrusion testing

A pure extrusion test was used to benchmark and compare the extrusion performance of the modified and standard nozzles. Custom g-code was written which instructed the printer to extrude exactly 1200 mm of raw filament into open space without printhead movement. The mass of extruded material was measured and used to calculate extrusion percentage at each rate.

Extrusion percentage, the percentage of material extruded for each nozzle design against VFR is plotted in Figure 8a. All modified nozzles outperformed the standard nozzle, with the 0.7 mm insert, bored nozzle performing the best of the five nozzles tested. Die swell ratio, the ratio of extruded diameter to nozzle orifice diameter is plotted for each nozzle design, see Figure 4b. The standard nozzle displays a linear and significant increase in diameter with VFR when compared to the modified nozzles which show small and near identical increases. Figure 4c depicts flow at 5 mm³/s and 8d at 20 mm³/s for the standard nozzle showing a substantial increase in diameter and swelling. The figure also demonstrates inconsistency in flow at higher VFRs, indicating flow effects (such as turbulence) are affecting the quality of flow.

https://doi.org/10.1017/pds.2023.303 Published online by Cambridge University Press

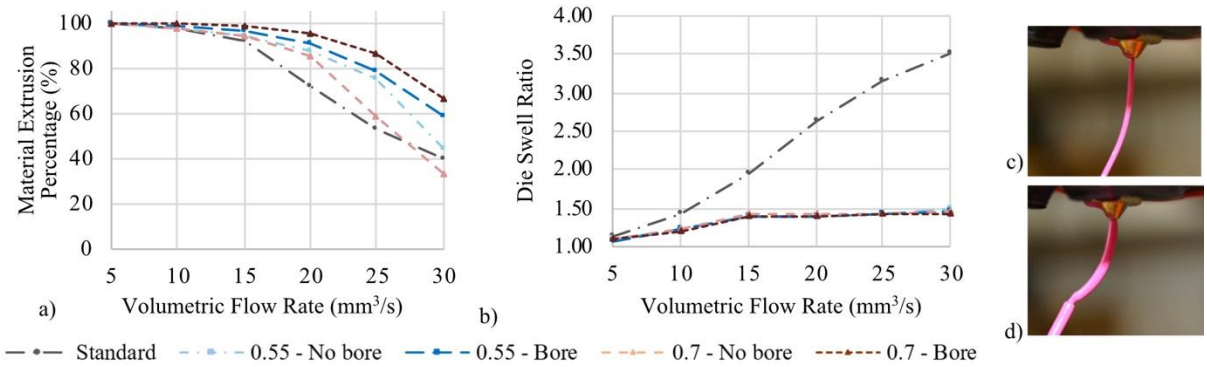

Figure 4. Graphs displaying a) extrusion percentage and b) diameter increase against VFR. Images of flow through standard nozzle at c) 2 mm³/s and d) 20 mm³/s.

Analysis of Figure 4a shows that, for the modified nozzles, the bored nozzles outperform their unbored equivalents. This indicates that the cross-sectional area of the nozzle bore was an important parameter to control. The 0.7 mm insert bored nozzle outperforms the 0.5 mm insert bored nozzle, suggesting the thicker insert benefitted the heating process. This is likely due to its ability to conduct heat to the surface at a quicker rate than the 0.5 mm insert as there is a larger volume of material to hold and transfer heat, the only variable between these nozzles. This effect was not considered within the analytical method, which may impact the results.

Figure 4b presents a marked improvement (reduction) in the die swelling for all the modified nozzles, relative to the conventional nozzle. As discussed, this should have a direct improvement on the quality of the fabricated artefact. Further visual checks were performed to assess if the filament displayed any turbulent characteristics on exit of the nozzle. A small amount of flow inconsistency (similar to that in Figure 4d was evident for the modified nozzles, seen as a slightly uneven flow on exit of the nozzle. This was likely caused by roughness in the internal geometry. However, the uneven flow was not significant and would not be expected to notably effect print quality.

Figure 4b illustrates a near inverse linear relationship between the die swell ratio and VFR, and thereby temperature, for the standard nozzle. This relationship is supported by existing literature (Liang, 2008). The small variation of die swelling with increase in VFR for the modified nozzles (see Figure 4b) indicates that the outlet temperature of the filament does not significantly varying between nozzle designs or as VFR increases. This suggests that temperature is not the primary limiting factor of the modified nozzle's ability to extrude material at high VFRs. Instead, a restriction in the flow, due to the additional internal geometry, is likely the limiting factor.

4.2 Print quality and speed

To examine print quality and speed, a custom meandering pathway was designed which incorporated sharp corners, curves, and a relatively long straight portion. The sharp corner tested the printers' motor abilities to change direction suddenly without compromising quality of print. The curves tested layer adhesion and internal stresses as the curvature makes the filament tend to a straight and shorter path. The long straight portion ensures the printhead reaches the maximum speed if not met on curved and corner portions. Failure would manifest itself as gaps in the laid filament or thinner extrusion width due to under extrusion. Custom G-code in Prusa Slicer was written to increase printer speed every 5 mm, in Z axis, at 5 mm³/s increments (from 5 mm³/s to 30 mm³/s). The spiral vase setting in Prusa Slicer (Prusa, no date) was used to produce quick and continuous prints with one perimeter and no infill or supports.

The print quality test was performed for each nozzle. All modified nozzles showed an improvement in print speed compared to the standard nozzle whilst maintaining print quality. Images of the meandering paths were taken to visually monitor when and what type of failure occurred for each nozzle. Figure 5a-c show the meandering path for the standard nozzle focusing on the curved, sharp, and straight portions respectively. Similarly, in Figure 5d, e and f for the bored 0.7 mm modified nozzle. Comparison of the figures show significant improvement in print quality performance at higher VFRs for the best performing modified nozzle compared to the standard. Figure 5d-e show no significant failure of the modified nozzle other than a small amount of under extrusion. In contrast, Figure 5 a-c shows significant failure at much lower VFRs. A refined experimentation and observation

https://doi.org/10.1017/pds.2023.303 Published online by Cambridge University Press

of the failure region for each nozzle showed an 86% increase in VFR was possible using the modified nozzle (26 mm^3/s compared to 14 mm^3/s).

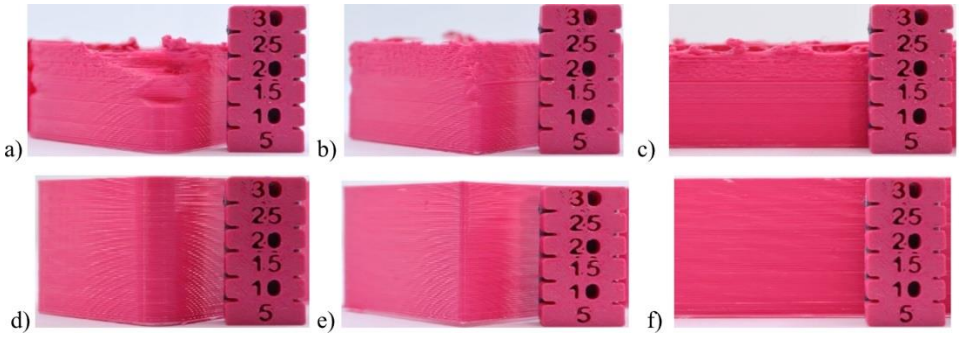

Figure 5. Images of curved corner, sharp corner and long straight line of meandering path using standard nozzle a) - c) and modified 0.7 mm insert bored nozzle d) – f) with gauge indicating corresponding VFR for each 5 mm section.

4.3 Use case application

To evaluate the benefit of the modification on the real-world fabrication of product prototypes, a study of the print times for the top 10 things on Thingiverse – a widely used design repository – was undertaken. The parts included 3D printer test parts, relatively large plant pots and drawers, and very small toys and utility pieces.

For comparison, the Prusa Slicer default "draft" setting was used, the expected quality used for early prototypes, along with a modified version of the parameters that accounted for the increased extrusion rate now achievable. Table 1 summarises the results, where it was found that a mean ~22.8% print time improvement was possible, equivalent to ~43 minutes per part. This is the equivalent of 1-2 additional prototypes being fabricated in a workday – demonstrating significant prototype fabrication efficiency improvement.

Table 1. Manufacturing times, for the ten most popular products on Thingiverse, using Prusa default and modified settings.

Part	Conventional Print Time (Minutes)	Modified Print Time (Minutes)	Absolute Difference (Minutes)	Relative Difference (Conventional baseline)
3D Benchy	38	34	-4	-10.5%
Whistle	43	32	-11	-25.6%
Solar Clock (Northern)	269	183	-86	-32.0%
Self-Watering Plant Pot (Both Parts)	328	170	-158	-48.2%
Modular Arm - Base	48	37	-11	-22.9%
Headphone Stand	247	207	-40	-16.2%
Filament Clamp Octave	2	2	0	0.00%
Hive Drawer + Module	257	181	-76	-29.6%
Octopus (V6 with Support)	87	67	-20	-23.0%
Printer Test 3rd Generation	121	97	-24	-19.8%
Mean	144	101	-43	-22.8%

One part that did not show a significant improvement was the filament clip. This is due to its small volume and length, thus not allowing the printer to accelerate to the maximum deposition rate in either

https://doi.org/10.1017/pds.2023.303 Published online by Cambridge University Press

setup. Still, averaged over the entirety of the considered parts, the improvement from the modification is generally applicable to the most fabricated forms.

5 DISCUSSION

Both the analytical and experimental results have shown that a print speed performance improvement can be achieved. When comparing the analytical and experimental results for each design method, results for the standard nozzle showed good agreement, suggesting that the assumptions around constant wall temperature and laminar flow were reasonable. However, for the modified nozzle, a ~45% discrepancy was observed in the worst instance (0.5 mm nozzle, unbored). One possible reason for this is that the insert causes turbulence in the material flow, thus assumptions around laminar flow are no longer reasonable. Additionally, it has been shown in Section 4.1 that the constant temperature boundary condition applied to the insert was likely a source of error. The 0.7 mm insert experimental results better correlation with the analytical than the 0.5 mm insert, likely due to increased volume and thermal inertia, further supporting this hypothesis.

Overall, there appears to be a significant improvement in VFR, though it is recognised that flow restriction may now be a limit factor. The likely cause of this restriction is the inlet insert shape (which was a somewhat arbitrary in this work) and the profile of end of the insert (which was a square section). Inspiration may instead be taken from low drag aerofoils, which have a smoother frontal area and reduce to a point downstream. This should improve the VFR further and improve the consistency of flow.

To appraise the impact of the increased VFR on the printing process, the fabrication times of common parts was evaluated. This revealed a substantial reduction in the fabrication time of prototypes (shown within Section 4.3 to be ~23% for a selection of popular parts), which in turn means that the prototyping activity can be completed more quickly – improving the efficiency of the prototyping and design process. Based on an eight-hour working day and the ten most downloaded artefacts, the increased rate would allow an extra prototype iteration to be completed each day.

The effect of this improvement would reduce with slower depositions – often used when trying to print with higher quality – but at that stage the movement system of the machine is the limiting factor. As such, future work may look at improving the accuracy and speed of the machine(s) to improve print speed for a wider quality range. This would additionally enable MEX printing for use in large-volume and mass manufacture applications, beyond that already undertaken.

The improvement in print speed will further improve energy consumption in the fabrication of prototypes and other parts. Although the hot end itself may be run at a lower temperature, as the energy can now be better transferred to the filament, this often makes up only a small part of the total energy used in the print process. Instead, the reduction in print time is likely to have a more significant effect through reducing the time the print bed – often heated to ~60 °C for PLA printing to improve bed adhesion – can be reduced. Although the temperature for the print bed is lower, the greater thermal inertia and cooling the print bed experiences causes this to be the more demanding process. There is currently estimated to be ~250,000 MEX 3D printers in the UK in 2021 (3D Printing Waste, no date), with a MEX printer estimated to use around 70 W whilst printing PLA (Dwamena, no date). This is equivalent to 420,000 kWh per day of printing PLA. As such, if fabrication time (and therefore how long the printers are operating for) can be reduced by ~23%, a saving of up to ~95,760 kWh per day of printing can be achieved.

It is recognised that the reported improvements are all dependent upon the geometry that is being printed. In some instances, there may be no improvement in the fabrication time of the part. This is generally when the part has many changes in direction – meaning the printer cannot accelerate up to the maximum deposition speed – or when the part is very small, and the shell and first layer make up a larger percentage of the fabrication (as these are generally printed slower). However, for other parts – namely for those with large radius curves and minimal sudden changes in direction – it is possible to decrease print time by up to ~50 % (see the plant-pot example in Table 1). For this reason, more careful consideration of Design for Additive Manufacturing (DfAM) rules may need to be considered in the design of either end use parts and/or prototypes for MEX manufacture using the method. Although entire parts are unlikely to be modified to improve the fabrication of one of their prototypes, it may be possible to fabricate small sections more rapidly by making small geometry changes to favour DfAM.

https://doi.org/10.1017/pds.2023.303 Published online by Cambridge University Press

6 CONCLUSION AND FUTURE WORK

The aim of this paper was to investigate how print time in material extrusion 3D printing for the purposes of prototyping could be reduced via modification (improvement) of an existing sub-system. Current solutions and limiting parameters were established and reviewed. The hotend sub-system was selected for modification. The limitation of this sub-system was found to be a volumetric flow rate of approximately 14 mm^3/s through the nozzle, established through analytical and experimental methods which showed a strong correlation. An improvement to the performance limitation of the sub-system was successful, through nozzle modification, achieving an 86% increase in maximum VFR.

The effect of the improvement on print time for a range of popular consumer parts were also considered. In the best instance, it was found that a print time improvement of approximately 48% could be achieved, with a mean of ~23% across all 10 parts. It was found that the magnitude of improvement was related to the geometry of part being printed, with greater benefits determined for parts with regions of large continuous depositions. Conversely, small intricate parts requiring many changes in direction demonstrated reduced gains due to the print head moving slower than its ultimate printing speed for relatively long periods. As such, it is recognised that the new limiting sub-system is likely to be the movement of the printer, and so further work may investigate improvements within this area.

The demonstrable improvement in print speed correlates to improving prototyping rate and efficiency, which should thereby improve the design cycle efficiency. In real terms, it was identified that a potential 1 or 2 extra prototypes may be possible in a working day without any other process modifications. Although this discounts time for use and interaction with the prototype, there is significant benefit to this when printing multiple iterations in a short timeframe for comparative testing (such as user-centred design). Additionally, there is sizeable benefit for short-run production, mass manufacturing, and large-scale 3D printing outside of prototyping activities. Benefit was further demonstrated in the energy use of the printer, with potential savings of ~23% energy use (equivalent of up to 100,000 kWh per day across the UK).

Future work should look at improving the flow effects caused by the insert, as well as how the insert is contained within the nozzle (both how the slot is cut and how it is retained). This would improve the maximum VFR achievable, as well as improve the consistency in flow. Future work may also look at improving the accuracy of the analytical model, likely by considering the non-laminar flow, removing the constant temperature boundary condition for the insert, and/or modelling in three dimensions.

ACKNOWLEDGMENTS

The work reported in this paper has been undertaken as part of the Twinning of digital-physical models during prototyping project at the University of Bristol, which is funded by the Engineering and Physical Sciences Research Council (EPSRC), grant reference (EP/R032696/1).

REFERENCES

3D Printing Waste (no date) '3D Printing Waste'. Available at: https://3dprintingwaste.co.uk/about-us/ (Accessed: 25 November 2022).

Anderegg, D.A. *et al*. (2019) 'In-situ monitoring of polymer flow temperature and pressure in extrusion based additive manufacturing', Additive Manufacturing, 26, pp. 76–83. Available at: https://doi.org/10.1016/j.addma.2019.01.002.

Ansys (no date) 'ANSYS FLUENT 12.0 User's Guide'. Ansys (12. Using the Solver). Available at: https://www.afs.enea.it/project/neptunius/docs/fluent/html/ug/main_pre.htm (Accessed: 20 March 2022).

Bondtech CHT® Coated Brass Nozzle (no date) Bondtech. Available at: https://www.bondtech.se/product/bondtech-cht-mk8-coated-brass-nozzle/ (Accessed: 12 March 2022).

Brooks, H., Rennie, A. and Abram, T. (2020) 'Variable fused deposition modelling- concept design and tool path generation', in. Available at: https://doi.org/10.13140/2.1.2280.2887.

BSI (2021) Additive Manufacturing - General principles - Fundamentals and vocabulary. BSI Standards Publication.

Camburn, B. *et al*. (2017) 'Design prototyping methods: state of the art in strategies, techniques, and guidelines', Design Science, 3, p. e13. Available at: https://doi.org/10.1017/dsj.2017.10.

Dwamena, M. (no date) 'How Much Electric Power Does a 3D Printer Use?', 3D Printerly. Available at: https://3dprinterly.com/how-much-electric-power-does-a-3d-printer-use/ (Accessed: 25 November 2022).

E3D (2022) Volcano HotEnd. Available at: https://e3d-online.com/products/volcano-hotend (Accessed: 28 November 2022).
Felton, H., Yon, J. and Hicks, B. (2020) 'Looks like but does it feel like? Investigating the influence of mass properties on user perceptions of rapid prototypes', Proceedings of the Design Society: DESIGN Conference, 1, pp. 1425–1434. Available at: https://doi.org/10.1017/dsd.2020.111.
FilaPrint (no date) FilaPrint Magenta Premium PLA 1 75mm 3D Printer Filament. Available at: https://shop.3dfilaprint.com/ (Accessed: 17 March 2022).
Go, J. *et al*. (2017) 'Rate limits of additive manufacturing by fused filament fabrication and guidelines for high-throughput system design', Additive Manufacturing, 16, pp. 1–11. Available at: https://doi.org/10.1016/j.addma.2017.03.007.
Hallgrimsson, B. (2012) Prototyping and Modelmaking for Product Design. Laurence King Publishing. Available at: https://books.google.co.uk/books?id=2QyeuAAACAAJ.
Hamad, K., Kaseem, M. and Deri, F. (2011) 'Melt Rheology of Poly(Lactic Acid)/Low Density Polyethylene Polymer Blends', Scientific Research, p. 7. Available at: https://doi.org/10.4236/aces.2011.14030.
Liang, J.Z. (2008) 'Effects of extrusion conditions on die-swell behavior of polypropylene/diatomite composite melts', Polymer Testing, 27(8), pp. 936–940. Available at: https://doi.org/10.1016/j.polymertesting.2008.08.001.
Mackay, M.E. (2018) 'The importance of rheological behavior in the additive manufacturing technique material extrusion', Journal of Rheology, 62(6), pp. 1549–1561. Available at: https://doi.org/10.1122/1.5037687.
Mishra, A.A. *et al*. (2021) 'Implementation of viscosity and density models for improved numerical analysis of melt flow dynamics in the nozzle during extrusion-based additive manufacturing', Progress in Additive Manufacturing [Preprint]. Available at: https://doi.org/10.1007/s40964-021-00208-z.
Moldex (no date) 'Moldex 3D R16 Support Manual - Viscosity Model for Thermoplastic'. (Viscosity Model for Thermoplastic). Available at: http://support.moldex3d.com/r16/en/index.html **(Accessed: 8 February** 2022).
Phan, D.D. *et al*. (2020) 'Computational fluid dynamics simulation of the melting process in the fused filament fabrication additive manufacturing technique', Additive Manufacturing, 33, p. 101161. Available at: https://doi.org/10.1016/j.addma.2020.101161.
Prusa (no date) PrusaSlicer. Available at: https://www.prusa3d.com/page/prusaslicer_424/ (Accessed: 25 November 2021).
Prusa Research (2021) 'Original PRUSA I3 MK35S+'. Available at: https://shop.prusa3d.com/en/3d-printers/180-original-prusa-i3-mk3s-kit.html?gclid=CjwKCAjw-e2EBhAhEiwAJI5jgzl6xvBHh4hAwmkF0RZazJA89aGg9-jQ_4Mcxh7pO5lgTU_q9O9h7hoCl0YQAvD_BwE (Accessed: 12 May 2021).
P.Serdeczny, M., *et al*. (no date) 'Numerical modeling of the polymer flow through the hot-end in filament-based material extrusion additive manufacturing', 36. Available at: https://doi.org/10.1016/j.addma.2020.101454.
Redwood, B., Schöffer, F. and Garret, B. (2017) The 3D Printing Handbook: Technologies, Design and Applications. 3D Hubs B.V. Available at: https://books.google.co.uk/books?id=R3OvswEACAAJ.
Sculpteo (2020) The State of 3D Printing 2020, p. 23.
Sculpteo (2021) The State Printing of 3D Printing 2021.
Serdeczny, M.P. (2020) Numerical and Experimental Analysis of Filament-based Material Extrusion Additive Manufacturing. Denmark.
Shaqour, B. *et al*. (2021) 'Gaining a better understanding of the extrusion process in fused filament fabrication 3D printing: a review', The International Journal of Advanced Manufacturing Technology, 114(5–6), pp. 1279–1291. Available at: https://doi.org/10.1007/s00170-021-06918-6.
Vicente, J. de (2012) Viscoelasticity - From Theory to Biological Applications. Available at: https://doi.org/10.5772/3188.
Wang, K. (2012) Die Swell of Complex Polymeric Systems, Viscoelasticity - From Theory to Biological Applications. IntechOpen. Available at: https://doi.org/10.5772/50137.
Youmans, R.J. (2011) 'The effects of physical prototyping and group work on the reduction of design fixation', Design Studies, 32(2), pp. 115–138. Available at: https://doi.org/10.1016/j.destud.2010.08.001.
Zhang, J. *et al*. (2021) 'Temperature Analyses in Fused Filament Fabrication: From Filament Entering the Hot-End to the Printed Parts', 3D Printing and Additive Manufacturing, p. 3dp.2020.0339. Available at: https://doi.org/10.1089/3dp.2020.0339.
Zhang, X. *et al*. (2018) 'Large-scale 3D printing by a team of mobile robots', Automation in Construction, 95, pp. 98–106. Available at: https://doi.org/10.1016/j.autcon.2018.08.004.